Acta Crystallographica Section D
Biological Crystallography
ISSN 0907-4449

Protonation states of histidine and other key residues in deoxy normal human adult hemoglobin by neutron protein crystallography

Andrey Kovalevsky,[a]* Toshiyuki Chatake,[b] Naoya Shibayama,[c] Sam-Yong Park,[d] Takuya Ishikawa,[b] Marat Mustyakimov,[a] S. Zoe Fisher,[a] Paul Langan[a] and Yukio Morimoto[b]

[a]Bioscience Division, Los Alamos National Laboratory, Los Alamos, NM 87545, USA, [b]Kyoto University, Research Reactor Institute, Kumatori, Osaka 590-0494, Japan, [c]Jichi Medical University, Department of Physiology, Shimotsuke, Tochigi 329-0498, Japan, and [d]Protein Design Laboratory, Yokohama City University, 1-7-29 Suehiro, Tsurumi, Yokohama 230-0045, Japan

Correspondence e-mail: ayk@lanl.gov

Received 6 April 2010
Accepted 28 June 2010

The protonation states of the histidine residues key to the function of deoxy (T-state) human hemoglobin have been investigated using neutron protein crystallography. These residues can reversibly bind protons, thereby regulating the oxygen affinity of hemoglobin. By examining the OMIT $F_o - F_c$ and $2F_o - F_c$ neutron scattering maps, the protonation states of 35 of the 38 His residues were directly determined. The remaining three residues were found to be disordered. Surprisingly, seven pairs of His residues from equivalent α or β chains, αHis20, αHis50, αHis58, αHis89, βHis63, βHis143 and βHis146, have different protonation states. The protonation of distal His residues in the $\alpha_1\beta_1$ heterodimer and the protonation of αHis103 in both subunits demonstrates that these residues may participate in buffering hydrogen ions and may influence the oxygen binding. The observed protonation states of His residues are compared with their ΔpK_a between the deoxy and oxy states. Examination of inter-subunit interfaces provided evidence for interactions that are essential for the stability of the deoxy tertiary structure.

1. Introduction

Hemoglobin (Hb) has evolved as an efficient transport protein that delivers oxygen to tissues in oxygen-breathing animals. Binding of O_2 molecules to heme groups is cooperative and involves an equilibrium between low-oxygen-affinity T (tense) and high-oxygen-affinity R (relaxed) quaternary states, according to the Monod, Wyman and Changeux model (Monod *et al.*, 1965). The binding of allosteric (heterotropic) effectors, such as hydrogen ions (H^+), chloride anions (Cl^-), carbon dioxide and inorganic and organic phosphates, to sites other than heme groups decreases the affinity of hemoglobin for O_2 (Tsuneshige *et al.*, 2002; Yonetani *et al.*, 2002). The effects of these small ions and molecules on the T$\leftrightarrow$R equilibrium have been included in the famous stereochemical model of Perutz, which states that T$\leftrightarrow$R transitions are accompanied by both quaternary and tertiary conformational changes in Hb (Perutz *et al.*, 1987, 1998; Perutz, 1989). The interactions with H^+ are of particular interest because they are manifested in the dependency of Hb oxygen affinity on pH, which is called the Bohr effect (Wyman, 1964). At pH values above 6 the oxygen affinity in normal human adult Hb (HbA) increases and it peaks at pH 7.4. The magnitude of the Bohr effect is the number of extra H^+ ions bound to the deoxygenated HbA relative to the oxygenated HbA (Shih & Perutz, 1987; Rao & Acharya, 1992). This implies that the T state has a higher affinity for H^+ than the R state. The chemical groups

© 2010 International Union of Crystallography
Printed in Singapore – all rights reserved

that can take up and then release a proton during T↔R transitions are called the Bohr groups (Berenbrink, 2006). Accordingly, those amino-acid residues that have different pK_a values in the T and R states may contribute to the Bohr effect.

The HbA molecule consists of two α and two β chains assembled into $\alpha_2\beta_2$ tetramers, with each chain noncovalently holding a single heme molecule. The N-terminal main-chain amino groups of αVal1 and the imidazole side chains of some histidine (His) residues have been assigned Bohr-group status (Perutz, 1970; Riggs, 1988). HbA contains 38 His residues: ten in each α chain and nine in each β chain. Notably, some experimental work, including solution and crystallographic data, was in favour of βHis146, which is located at the C-termini of the β chains, participating almost exclusively in the Bohr effect, with insignificant contributions from the αVal1 amino groups, αHis20 and αHis89 (Perutz *et al.*, 1980, 1985; Cera *et al.*, 1988; Englander & Englander, 1987). In contrast, other measurements and also theoretical calculations pointed out that the Bohr effect is not confined to just a few amino-acid residues, but rather that it is global, traversing the whole HbA tetramer with contributions from many residues, and its magnitude may change if measured in different buffers (Ho & Russu, 1987; Russu *et al.*, 1989; Busch & Ho, 1990; Busch *et al.*, 1991; Matthew *et al.*, 1985). Solution 2D proton NMR measurements (Sun *et al.*, 1997; Fang *et al.*, 1999) and chemical reactivity (Rao & Acharya, 1992) studies further supported the concept of many sites participating in H^+ capture and release, including most His residues, the terminal amino groups and other proton-binding sites (*e.g.* βGlu43). The NMR spectra also demonstrated that residues contribute in either a positive or negative way to the overall Bohr effect, with their pK_a shifting to lower or higher values, respectively.

Most of our understanding of the function and allosteric regulation of HbA comes from X-ray crystallography and NMR studies. However, in order to elucidate the mechanism of the Bohr effect at the atomic level, the protonation states of amino acids in HbA have to be determined. X-rays are not well suited for direct imaging of H atoms, even at ultrahigh resolutions of better than 1 Å, while assigning peaks to particular H atoms in NMR spectra can be problematic, especially for a protein as large as HbA. To date, the pK_a values and shifts of only 24 His residues are known (Sun *et al.*, 1997; Fang *et al.*, 1999). In contrast, H atoms and even H^+ ions can be straightforwardly imaged by neutron crystallography (Blakeley *et al.*, 2008). Neutrons are scattered by atomic nuclei, rather than electron clouds as in the case of X-rays, and therefore the scattering power of an atom is not dependent on its atomic number. The hydrogen isotope deuterium (D), carbon and oxygen have similar scattering lengths, while hydrogen scatters neutrons with a negative scattering length (http://www.ncnr.nist.gov/resources/n-lengths/list.html). Thus, the great advantage of neutron diffraction is that heavy atoms and deuterium in a protein appear as strong positive peaks in the nuclear scattering density maps, while hydrogen is observed as negative troughs and can easily be distinguished from deuterium. A detailed review of structures determined using the neutron diffraction method has recently been published (Blakeley, 2009). We therefore pursued neutron diffraction studies of HbA. We developed a crystallization technique that allowed us to produce crystals of deoxy-HbA of 20 mm^3 in size. We collected neutron diffraction data using the Protein Crystallography Station (PCS) at Los Alamos Neutron Science Center (Los Alamos National Laboratory, Los Alamos, New Mexico, USA) in order to directly determine the protonation states of putative Bohr groups. The current neutron structure of deoxy-HbA was obtained at 2 Å resolution. In our previous analysis, based on data collected with monochromatic neutrons from a reactor, the protonation states of 20 His residues could be determined (Chatake *et al.*, 2007). However, the insufficient resolution (2.1 Å) and completeness of those data did not allow us to establish the protonation states of the remaining His residues. With the current improved data, we could unambiguously assign the protonation states of 35 of the 38 histidines and other ordered residues. The current results are presented here in comparison with our previous neutron crystallographic study and the earlier 2D NMR measurements.

2. Materials and methods

2.1. Crystallization of deoxy-HbA and sample preparation

Hemoglobin was purified from human blood according to published procedures (Shibayama *et al.*, 1991). It was transferred into D_2O buffer to initiate H/D exchange and a large 20 mm^3 crystal was grown by the batch method using previously published methodologies (Chatake *et al.*, 2007; Kovalevsky *et al.*, 2008). The crystal was sealed under anaerobic conditions in a quartz capillary containing the D_2O mother liquor to allow further H/D exchange, an oxygen absorber and an oxygen indicator.

2.2. Neutron crystallographic data collection, structure determination and refinement

46 diffraction images were collected using the TOF Laue neutron diffractometer at PCS (Langan *et al.*, 2004, 2008) with 12 h exposure time per image. The intensities of the reflections were measured using a version of *d*TREK* (Pflugrath, 1999) modified for TOF data analysis (Langan *et al.*, 2004), wavelength-normalized with *LAUENORM* (Helliwell *et al.*, 1989) and then merged with *SCALA* from the *CCP*4 suite of programs (Collaborative Computational Project, Number 4, 1994), giving an overall completeness of 86.7% to 2.0 Å resolution. The current neutron structure was refined with *nCNS* (Adams *et al.*, 2009), starting with the coordinates from the previous neutron structure (PDB entry 2dxm; Chatake *et al.*, 2007). A combination of rigid-body, positional, individual temperature-factor and individual occupancy refinement was used. 299 water molecules were picked from peaks higher than 2σ in the neutron $|F_o| - |F_c|$ Fourier map and refined as D_2O molecules. At the final stages of the refinement, the level of H/D exchange of the labile main-chain amides was refined. Finally, the protonation states of the side chains of His, Glu,

Asp, Tyr, Thr, Ser and Trp residues were determined by calculating neutron $2F_o - F_c$ and $F_o - F_c$ maps with no D atoms attached at the labile-atom positions. The negative neutron $2F_o - F_c$ maps were also examined to locate negative peaks representing non-exchangeable H atoms and to verify the correct conformations of the side chains. The resolution of the current 2 Å data is not sufficient to discuss the individual occupancies of D atoms on the side chains; thus, we did not refine them. In addition, we took great care interpreting the nuclear density maps in order to avoid any over-interpretation of the low-resolution data. For detailed crystallographic and refinement statistics, the reader is referred to Table 1 of Kovalevsky *et al.* (2010).

2.3. Hydrogen/deuterium-exchange (HDX) analyses

An analysis of the HDX pattern was carried out using recently reported methods (Bennett *et al.*, 2008). The *DPX* algorithm was used to calculate atom depth (Pintar & Pongor, 2003), where the depth of a main-chain N atom is defined as the distance to the closest atom that has a solvent-accessible surface. Surface amides have a zero value for the depth. The level of HDX decreases on average with the atom depth. The *CCP*4 program *NCONT* (Collaborative Computational Project, Number 4, 1994) was used to calculate hydrogen-bond parameters. The level of HDX increases on average with longer hydrogen bonds made by the main-chain amides.

3. Results and discussion

3.1. Neutron structural analysis

The current neutron structure (PDB code 3kmf; Kovalevsky *et al.*, 2010) of deoxy-HbA was refined in space group $P2_1$ using data to 2 Å resolution, with the whole tetrameric hemoglobin molecule occupying the asymmetric unit. There was clear nuclear density for the majority of the residues, the exceptions being a few highly disordered Lys or Glu side chains. The final model is superimposable with the previous neutron structure (PDB code 2dxm) and the 1.25 Å resolution room-temperature X-ray model (PDB code 2dn2; Park *et al.*, 2006), with the r.m.s. deviations on main-chain atoms being 0.3 and 0.4 Å, respectively. A detailed structural comparison of these three structures has been published elsewhere (Kovalevsky *et al.*, 2010). The most important outcome of the analysis is that the side chains of some His residues have different conformations in the three structures. Seven ordered His residues (α_1His72, α_1His89, β_1His77, α_2His72, α_2His89, β_2His97 and β_2His146) assume different conformations in the 3kmf and 2dn2 structures through a 180° flip of the imidazole ring. Of these, the side chains of α_1His72, α_1His89, α_2His72 and β_2His146 have poor electron density, whereas the corresponding nuclear density is strong and explicit. Conversely, β_1His77, α_2His89 and β_2His97 are adequately observed in both structures. However, the distinction between N and C atoms cannot be made and H atoms are not visible in the electron density at 1.25 Å resolution, making the interpretation of the imidazole-ring orientation challenging. The positive and negative nuclear density peaks for D and H make the determination of the imidazole-ring conformation unmistakable in the neutron structure (Fig. 1). A 180° flip of the imidazole rings distinguishes the conformations of α_1His72 and α_1His89 in the two neutron structures 3kmf and 2dxm. The rotational conformers of these residues could not be pinned down in 2dxm, which is likely to be a consequence of the lower resolution and completeness of the previous neutron data, while we have overcome this problem with the current neutron TOF experiment.

3.2. HDX analyses

It is instructive to discuss the backbone H/D-exchange pattern for the main-chain amide groups in HbA. The scattering length of H is −3.739 fm and that of D is 6.671 fm. Thus, the refined occupancy ranging between −0.56 and 1.00 of each D atom connected to a main-chain N atom provides us with the extent of D exchange for H. Fig. 2 depicts the level of HDX for each HbA chain. The residues are grouped into three categories, non-exchanged, partially exchanged and fully exchanged sites, with D occupancy ranges of −0.56–0, 0–0.6 and 0.6–1.0, respectively. Overall, the four chains show high levels of HDX. The HDX values averaged over the tetramer correlate well with the atomic depth of the main-chain N atoms computed using the *DPX* algorithm (Pintar & Pongor, 2003), although the r.m.s. deviations from these averages are large, as demonstrated by the error bars in Fig. 3(*a*). The r.m.s.d. values demonstrate that amides with depths of ∼3 Å can still undergo almost full H/D exchange, whereas those with depths of over 4 Å can at best be partially exchanged. The latter amides constitute the solvent-inaccessible hydrophobic

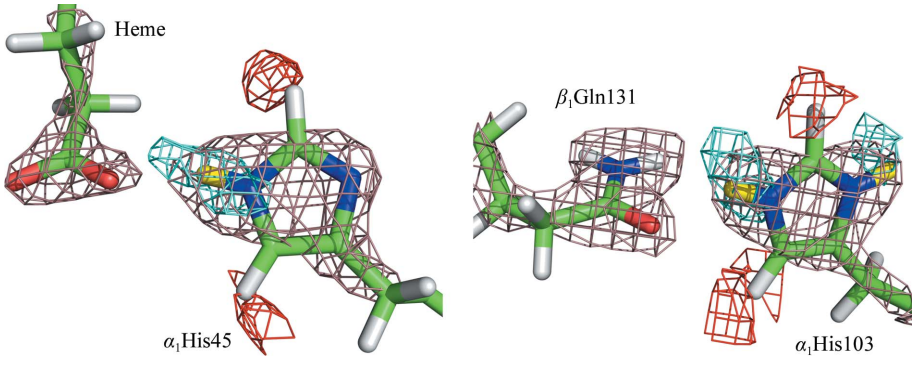

Figure 1
Examples of OMIT $F_o - F_c$ (cyan, contoured at the 2σ level), positive $2F_o - F_c$ (brown, contoured at the 1.6σ level) and negative $2F_o - F_c$ (red, contoured at the 1σ level) nuclear density maps for His residues that illustrate how the protonation states and orientations were determined. Peaks in OMIT $F_o - F_c$ maps unequivocally show the locations of D atoms, whereas peaks in the negative $2F_o - F_c$ maps demonstrate the positions of H atoms.

cores, shown in Fig. 2 as a stick representation surrounded by a half-transparent surface. It can be seen that the cores of the $\alpha_2\beta_2$ heterodimer are completely screened from solvent, whereas in the $\alpha_1\beta_1$ heterodimer they are not and have an HDX of ∼30%. From Fig. 3(*b*) there appears to be a correlation between HDX and hydrogen-bond distance: the shorter the hydrogen bond is, the less H/D exchange occurs. Again, the spread is considerable; a hydrogen bond of any distance can in principle incorporate a fully exchanged amide. However, the trend for the HDX to be less variable is obvious for the longer hydrogen bonds (Fig. 3*b*).

3.3. Protonation states

The protonation states of the putative Bohr groups αVal1 and βGlu43 could not be determined in the current analysis owing to their high disorder. The protonation states of 35 His residues could be unequivocally determined, as summarized

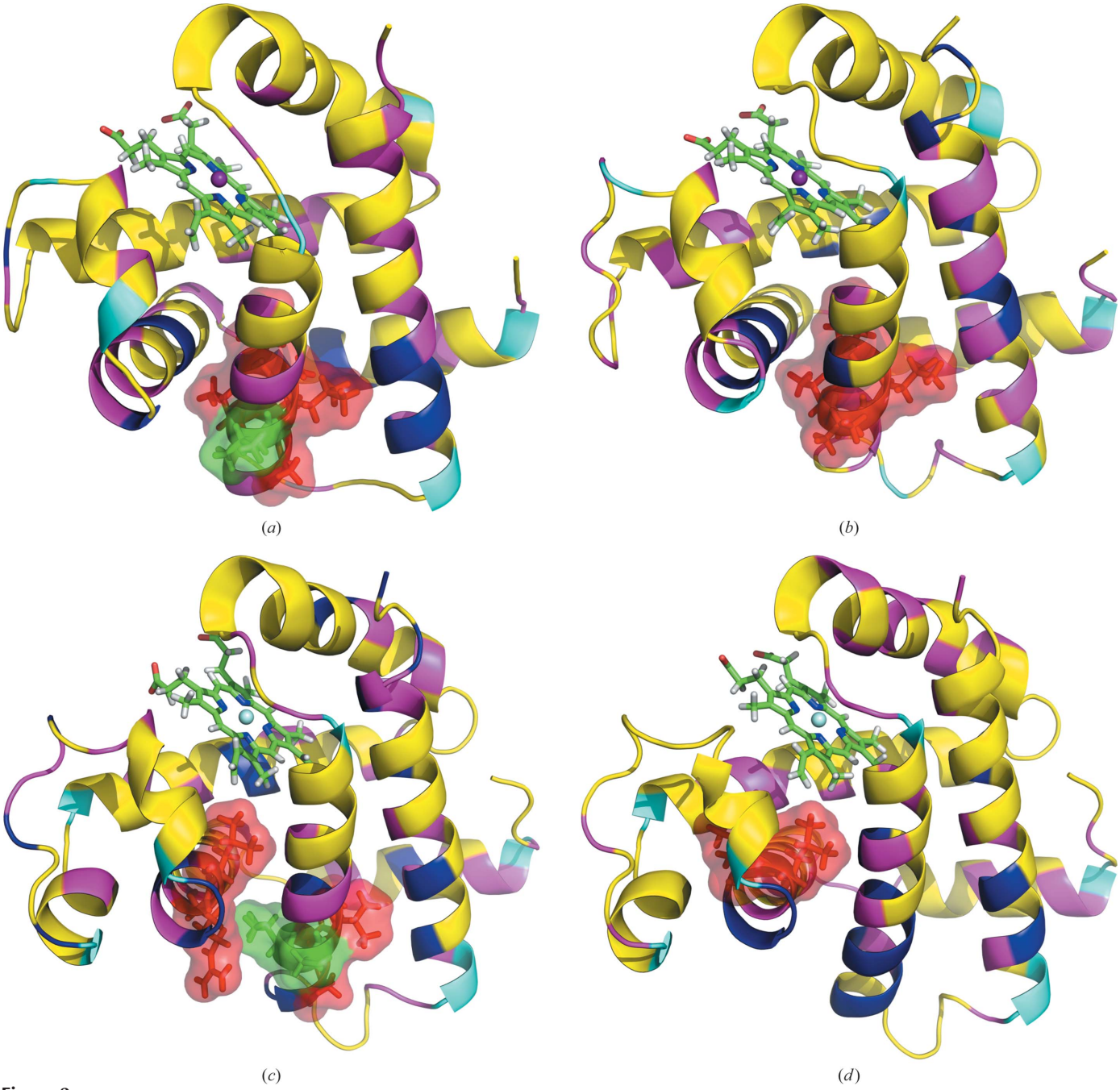

Figure 2
Backbone H/D-exchange patterns for the HbA molecule depicted in cartoon representation: (*a*) α_1, (*b*) α_2, (*c*) β_1 and (*d*) β_2 subunits. Yellow corresponds to fully exchanged, magenta to partially exchanged and blue to non-exchanged main-chain amides. Proline residues are shown in cyan. Heme groups are shown as sticks, while Fe ions are shown as purple and cyan spheres. Hydrophobic cores identified from HDX data and depth calculations are shown as semi-transparent surfaces and with side chains. The cores are the backbone amides with depths of >3 Å. A core is considered to be two or more residues at sufficient depth. Exchanged core residues are depicted in green, whereas non-exchanged core residues are shown in red.

previously by Kovalevsky *et al.* (2010), by inspecting OMIT $F_o - F_c$ and $2F_o - F_c$ nuclear density maps (Fig. 1). Positive density peaks in these maps near imidazole $N^{\delta1}$ and/or $N^{\varepsilon2}$ atoms indicated the presence of D atoms. We also accurately determined the rotational orientations of the imidazole side chains by examining negative $2F_o - F_c$ density maps. Negative density reveals the positions of non-exchanged H atoms attached to C atoms (Fig. 1). Three residues, β_1His2, β_1His117 and β_2His2, were disordered and their protonation states could not be determined. In the current study at 2 Å resolution the presence of D atoms connected to $N^{\delta1}$ and/or $N^{\varepsilon2}$ atoms of His residues, but not their occupancies, could be identified. Thus, we could not quantify the partial protonation of those His residues described as protonated and positively charged. Such quantification of His protonations could only be performed at a resolution of 1.5 Å or better. As a result, we do not exclude the possibility that some of the protonated His residues may correspond to mixtures of two tautomers of the side-chain imidazole ring, *i.e.* when a D atom appears on either $N^{\delta1}$ or $N^{\varepsilon2}$. The superposition of these tautomers in the crystal would look like a protonated His, provided that their positions and conformations are exactly the same. We carefully examined the current neutron structure in the light of this possibility. It is important to note that chemical knowledge suggests the full presence of a D atom on an imidazole N atom when it makes an N—D···O hydrogen bond to avoid unfavourable close N···O contacts. Most protonated histidines make salt-bridge interactions and hydrogen bonds with main-chain or D_2O O atoms and thus are likely to be protonated at both N atoms (Fig. 1). Although this explanation is very plausible, it however is not sufficient to completely resolve the issue of overlapped imidazole tautomers.

The most surprising finding of the current study is that seven pairs of His residues exhibit different protonation states in equivalent chains, including the four surface residues αHis20 (charges: α_1, +1; α_2, 0), αHis50 (α_1, 0; α_2, +1), αHis89 (α_1, 0; α_2, +1) and βHis143 (β_1, 0; β_2, +1), the distal histidines αHis58 (α_1, +1; α_2, 0) and βHis63 (β_1, +1; β_2, 0) and the terminal βHis146 (β_1, +1; β_2, 0). The other surface histidines and the buried residues αHis103 and αHis122 have the same protonation states in corresponding α or β chains (Fig. 4). As mentioned above, one explanation is that some protonated His residues in the nonmatching pairs may be mixtures of tautomers. Nevertheless, considering hydrogen bonding, none of these should be viewed as overlapping tautomers. In contrast, the residues α_1His72, α_2His72 and β_2His97 (all protonated) that have been assigned the same protonation states in both globins may indeed be possible mixtures of tautomers because they lack hydrogen-bonding interactions

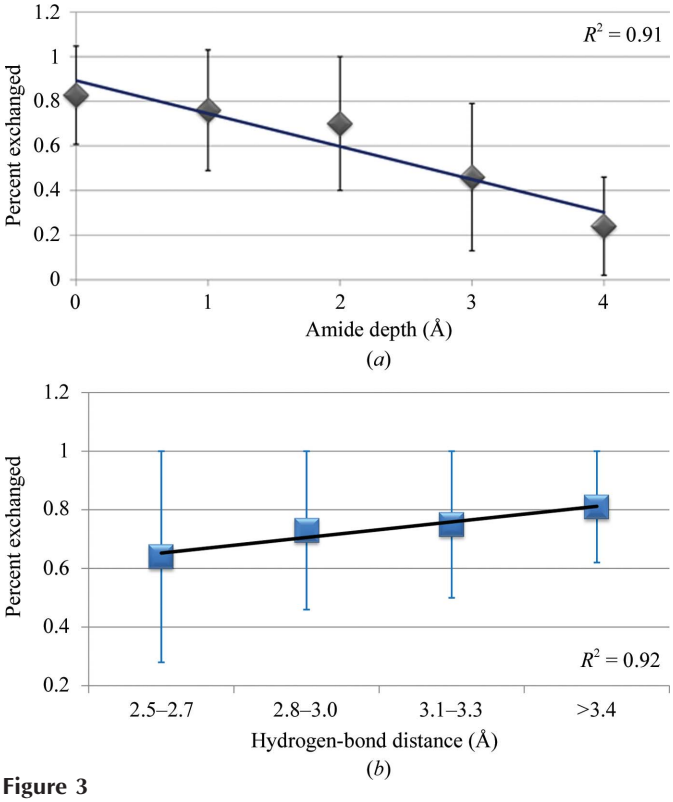

Figure 3
HDX analysis using the *DPX* algorithm. (*a*) Main-chain amide depth is plotted against H/D exchange for the tetramer of HbA; (*b*) hydrogen-bonding distance plotted against H/D exchange. The error bars are the calculated root-mean-square deviations (r.m.s.d.s) of the amide D occupancies for the groups of amides at a certain depth or within a certain hydrogen-bond range.

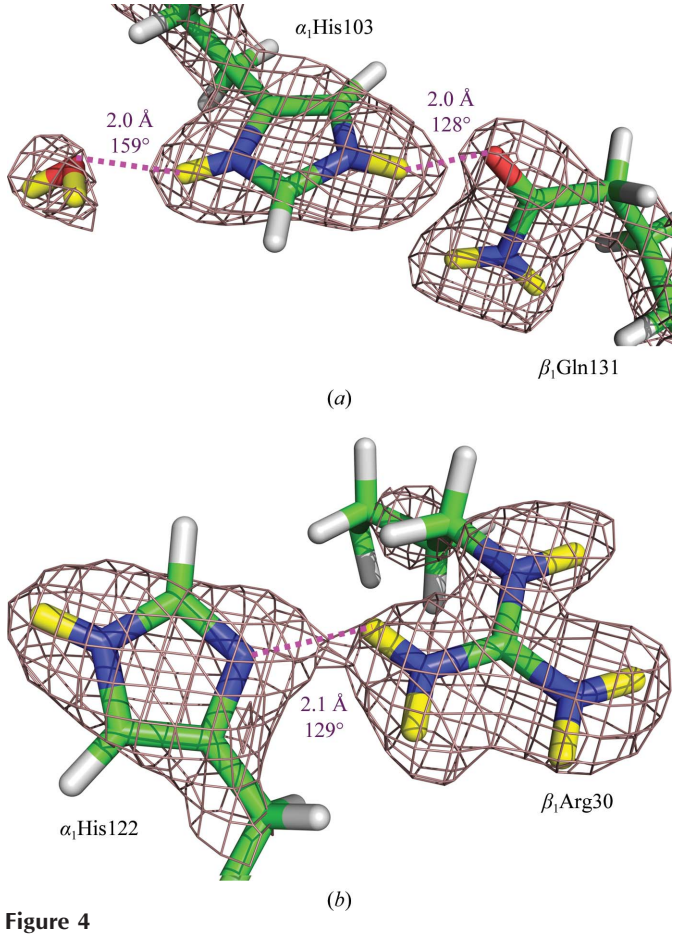

Figure 4
Protonation states and hydrogen bonding for the buried histidine residues α_1His103 (*a*) and α_1His122 (*b*). Nuclear density is contoured at the 1.5σ level. D···O and D···N distances and N—D···O and N—D···N angles for the hydrogen bonds are given.

with other residues or solvent molecules. Another explanation for the difference in protonation states is that the His pK_a values (Sun *et al.*, 1997; Fang *et al.*, 1999) are close to the pD of crystallization (6.7) and the surroundings may influence protonation and deprotonation. The pK_a values for αHis20, αHis50 and αHis89 were determined by NMR to be 7.23, 7.25 and 6.88, respectively. In addition, crystal-packing interactions may influence the protonation-state variations. The crystal environment may be involved for αHis20 and αHis89. The side chain of α_1His20 makes a salt bridge with the side-chain symmetry-related β_2Glu22, while α_2His20 is positioned in an empty cleft at least 8 Å away from the closest symmetry-related residue. The imidazole of α_1His89 does not make any interactions with symmetry-related atoms, but α_2His89 makes van der Waals contacts with the side-chain atoms of the symmetry-related β_1Ala76. The protonation of α_1His20 and α_2His89 may contribute to the crystal-packing stabilization energy. For the surface residues αHis50, βHis143 and βHis146 and also for the distal histidines αHis58 and βHis63 the crystal packing is unlikely to contribute to the protonation differences. In these cases, the symmetry-related atoms are over 6 Å away. Therefore, other factors as discussed below may play a dominant role.

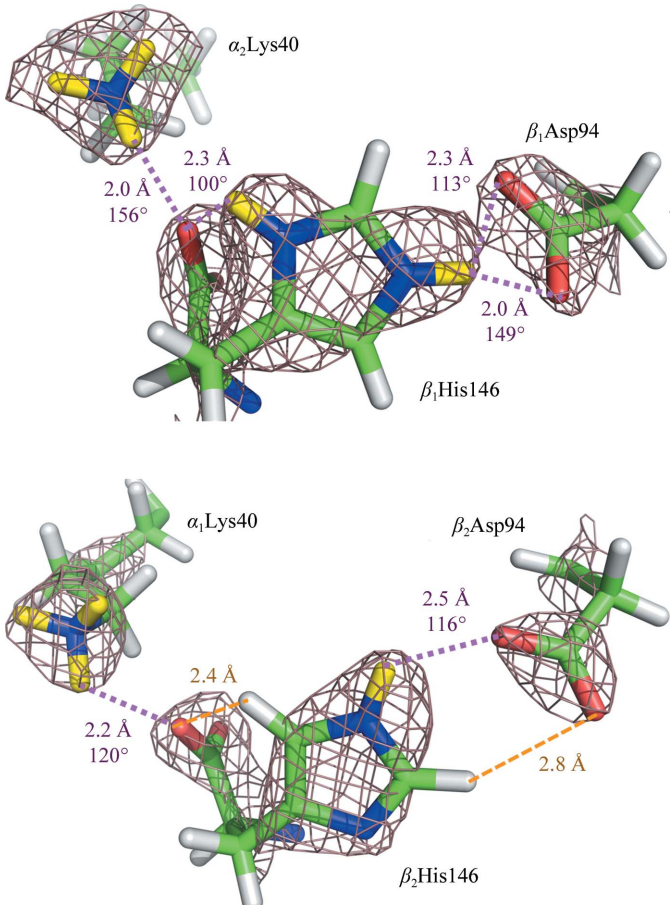

Figure 5
Protonation states and hydrogen bonding for the main-chain and side-chain groups of βHis146 in subunits β_1 and β_2. Nuclear density is contoured at the 1.5σ level. Hydrogen bonding is shown as magenta dotted lines, while the C—H···O contact between β_2His146 and the carboxylic moiety of β_2Asp94 is depicted as an orange dashed line. Nuclear density is contoured at the 1.5σ level. D···O distances and N—D···O angles for the hydrogen bonds and H···O distances for the C—H···O contacts are given.

We also compared the His protonation states in the current (3kmf) and previous (2dxm) neutron structures. The protonation states of only 20 histidines were determined in 2dxm, largely owing to the incompleteness of the neutron diffraction data (~70% overall and less than 50% for the highest resolution shell 2.2–2.1 Å; Chatake *et al.*, 2007). Surprisingly, six His residues differ in their protonation states between 3kmf and 2dxm. The surface histidines αHis72 and αHis112 are protonated in both subunits in the current structure, whereas they are all neutral in the previous structure. Slight variations in the crystallization conditions between 3kmf and 2dxm may have affected the charged states of these residues (the ΔpK_a of αHis112 is close to zero). In addition, the αHis72 residues may be mixtures of tautomers, as mentioned above. If this were correct, there would be no differences in αHis72 protonation between 3kmf and 2dxm. Differences in protonation for the distal His residues (α_2His58 and β_2His63) between the two structures cannot be attributable to the effects described above. The distal histidines were found to be protonated in all subunits in our previous neutron structure, but those in the $\alpha_2\beta_2$ heterodimer of the current structure are neutral. We explored the possibility that the completeness of the 2dxm neutron data played a role. However, a subset of reflections taken from the current data set that correspond to those used in the refinement of 2dxm produced the same protonation states as the full data set. Thus, we concluded that the incompleteness of the neutron data does not clarify the differences in the protonation states observed between the 3kmf and 2dxm structures. The surface and the distal residues are solvent-accessible (the amide depth is 0) and consequently can easily H/D-exchange. The level of HDX in the two structures should therefore be very similar and should not be a factor leading to protonation variations. Indeed, according to the DPX analysis most histidines are solvent-accessible, with depths ranging between 0 and 1.5 Å. Only the proximal and buried αHis122 residues have depths of around 3 Å. Our HDX analysis (Fig. 3*a*) demonstrates that, on average, residues with an amide depth of ~3 Å are 50% exchanged. As a result, we expect that all labile H atoms on His residues have undergone exchange with D.

The protonation states determined in the 3kmf structure for the $\alpha_1\beta_1$ heterodimer are consistent with those in 2dxm, while the protonation states in the $\alpha_2\beta_2$ dimer are not. In order to investigate this further, we determined the expected protonation states of His residues based on their ΔpK_a values calculated from the pK_a measured by NMR (Sun *et al.*, 1997; Fang *et al.*, 1999). For some histidines 2D NMR could not measure pK_a values in either or both of the deoxy and carbonmonoxy forms and thus their ΔpK_a are not known. Included in this group are the distal and buried His residues and also the surface residue αHis45. For αHis50 and βHis143 the ΔpK_a values are positive; the pK_a shift of the latter residue is not available under phosphate conditions similar to those used for crystallization. Accordingly, these two histidines have

to be neutral in order to accept an additional proton from the bulk solvent during oxygenation. The ΔpK_a values for βHis146 are negative and are the largest among all His residues independent of the buffer constituents; thus, they should be protonated in the T state. βHis146 is of great importance for stabilizing the T state (Perutz *et al.*, 1998) because it makes a salt bridge with the side-chain carboxylate of βAsp94 from the same subunit. This hydrogen bond is broken in the R state owing to the tertiary-structure changes in the T$\leftrightarrow$R transition. In 3kmf this hydrogen bond remains intact even though β_2His146 lacks an extra proton (Fig. 5). For three pairs the protonation states are reversed from what would be expected if the $\alpha_2\beta_2$ heterodimer were in the T state. As a consequence, and also taking into account the differences in protonation states of distal histidines, it would be reasonable to suggest that in the 3kmf structure the $\alpha_2\beta_2$ dimer may not be in a pure T state.

3.4. Distal His residues and comparison with myoglobin

The most noteworthy finding of the current study and our previous neutron structure is the determination of the protonation states of the distal histidines α_1His58, α_2His58, β_1His63 and β_2His63 and also of the buried residues. Solution methods were incapable of measuring pK_a values for these residues in the deoxy and oxy forms, thus the ΔpK_a values and their involvement in the Bohr effect have not been established. The pK_a values for the distal His in sperm whale deoxy-myoglobin was estimated by EPR to be ~5.4 (Ikeda-Saito *et al.*, 1977). If the pK_a did not change in deoxy-HbA, we would expect the αHis58 and βHis63 residues to be neutral, because the deoxy-HbA crystals were grown at a pD of 6.7. Yet, in the 3kmf structure the distal His side chains are protonated in the $\alpha_1\beta_1$ heterodimer and neutral in the $\alpha_2\beta_2$ heterodimer (Fig. 6). These histidines were found to be protonated in all chains in our previous 2dxm structure. Therefore, in deoxy-HbA the distal histidine pK_a values may be significantly higher than those in deoxy-myoglobin. In myoglobin, the distal His is located in a tight pocket capped by Arg45 and Thr67 (Yang & Phillips, 1996), while in HbA the distal His residues αHis58 and βHis63 are in pockets open to the bulk solvent, with only the conformationally flexible αLys61 or βLys66 located nearby. The presence of the positively charged Arg close to the distal His can substantially reduce the pK_a of the latter in

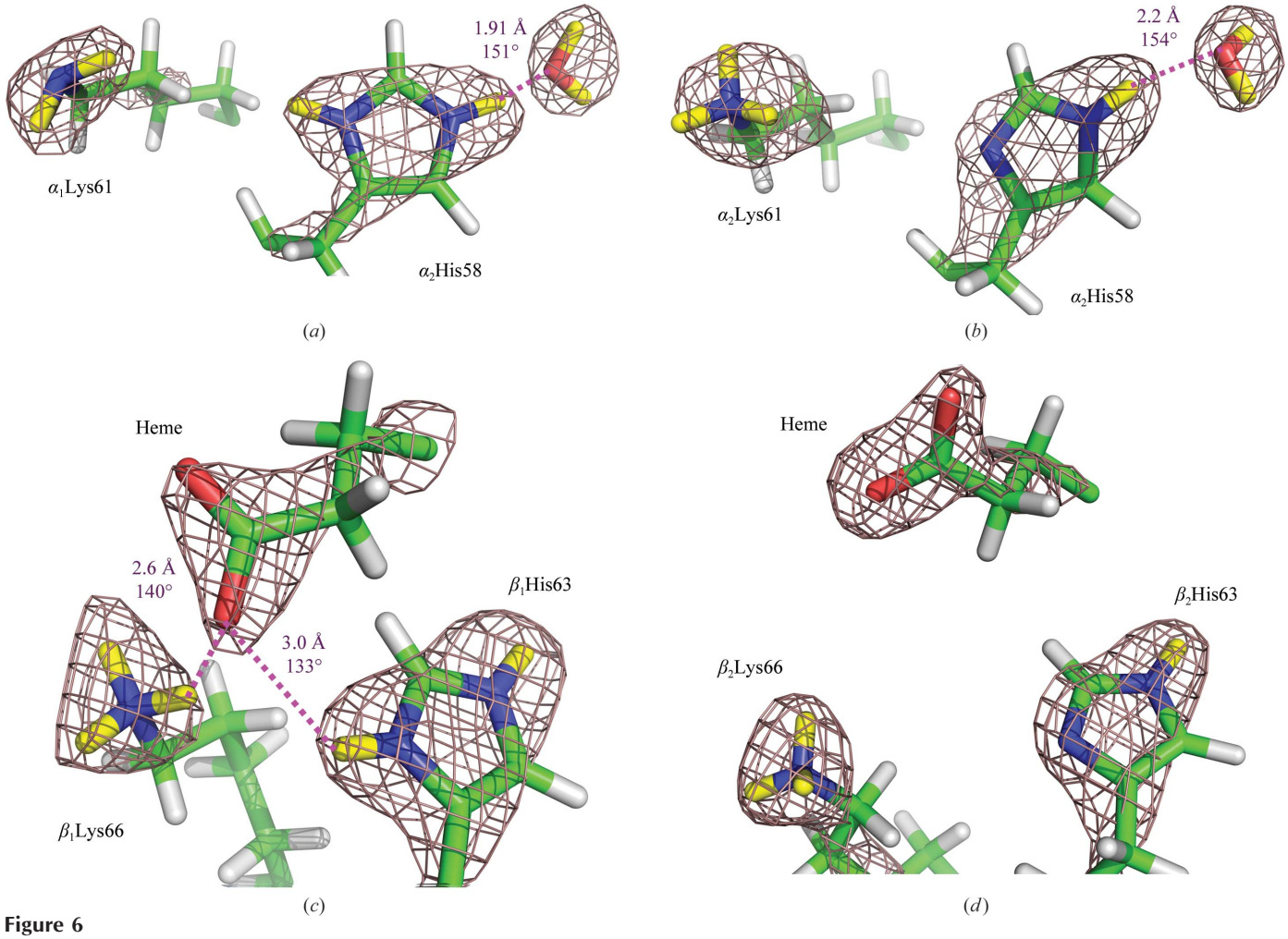

Figure 6
Protonation states and surroundings of and hydrogen bonds made by distal histidines. Nuclear density is contoured at the 1.5σ level. D$\cdots$O distances and N—D$\cdots$O angles for the hydrogen bonds are given.

myoglobin. X-ray crystallographic data (Yang & Phillips, 1996) have demonstrated that the distal His in myoglobin swings out and away from the heme in low-pH structures, where it is presumably protonated, leading to a shift of the Arg45 position towards the bulk solvent. We argue here that such reorientation of the distal histidines would not occur in HbA because of solvent accessibility and the lack of the second positive charge provided by arginine in myoglobin.

The His58 residues in α subunits are each hydrogen bonded to a D_2O molecule that lies only ∼3.3–3.5 Å away from the heme iron. These waters are held in place by $N^{\varepsilon 2}$—D···O and O—D···π interactions with imidazole and with the conjugated system of the heme, respectively. Their orientations could not be determined in the previous 2dxm structure. Importantly, these D_2O molecules do not alter their orientation as a result of the protonation or deprotonation of the histidine. These water molecules were also observed at the same locations in the published room-temperature X-ray structure of deoxy-HbA (PDB entry 2dn2; Park *et al.*, 2006). In both the α_2 and β_2 chains deprotonation results in the $N^{\delta 1}$ atom losing a D (Fig. 6). Fig. 6 also shows that conformational changes occur around distal His residues owing to deprotonation. In the $\alpha_1\beta_1$ heterodimer Lys61, which is located about 6 Å away from His58, is neutral and the protonated Lys66 and His63 residues make electrostatic interactions with the propionate of heme. On the other hand, in $\alpha_2\beta_2$ Lys61 is protonated and moved further away from the neutral His58. Similarly, deprotonation of β_2His63 caused the propionate of the heme and β_2Lys66 to swing away, thus losing the electrostatic contacts observed in the $\alpha_1\beta_1$ dimer.

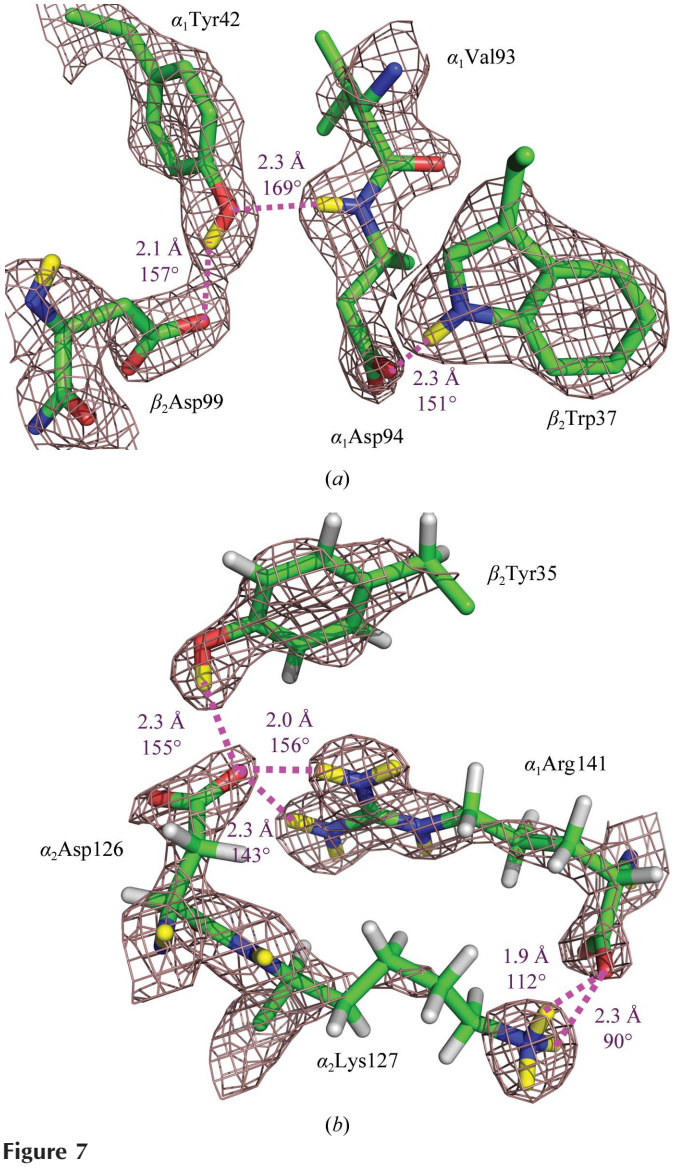

Figure 7
Protonation states and hydrogen bonding at the α_1–β_2 (*a*) and α_1–α_2–β_2 (*b*) interfaces. Nuclear density is contoured at the 1.8σ level. Hydrogen bonding is shown as magenta dotted lines. D···O and D···N distances and N—D···O and O—D···O angles for the hydrogen bonds are given.

3.5. Inter-subunit interactions

The current neutron structure provides valuable information on the interactions made between the subunits. Many of these contacts would disappear or diminish in the oxy form of HbA owing to the quaternary and tertiary changes associated with the transition to the R state. Salt bridges are made by the main-chain carboxylates of the βHis146 residues and the protonated ε-ND_3^+ groups of αLys40 in addition to the βHis146···βAsp94 hydrogen bonds (Fig. 5). The stability of the T-state tertiary structure at the C-termini of the β subunits is further enhanced by water-mediated interactions connecting these terminal carboxylic moieties to the main-chain carbonyl groups of α_2Pro37 and α_1Pro37. Several hydrogen bonds occur in the α_1–β_2 interfaces between α_1Asp94, β_2Trp37, α_1Tyr42 and β_2Asp99 and similarly between the α_2 and β_1 chains (Fig. 7*a*). The αAsp94 and βAsp99 residues are known to markedly influence the affinity of deoxy-HbA for hydrogen ions. Although their specific role has not been determined, site-directed mutagenesis studies have shown that α42 and β37 mutants are associated with a reduced Bohr effect (Imai *et al.*, 1991; Ishimori *et al.*, 1992). The hydrogen-bonding interactions within the α_1–α_2–β_2 and α_2–α_1–β_1 interfaces are also of note. These are created by both the main-chain and side-chain groups of the C-terminal αArg141 residues and the side chains of αLys127, αAsp126 and βTyr35, as depicted in Fig. 7(*b*). A salt bridge between the guanidinium group of the arginine and the carboxylate of αAsp126 disappears, while the salt bridge involving the main chain of the arginine and the side chain of αLys127 and a hydrogen bond between the carboxylic side chain of αAsp126 and the phenolic hydroxyl of βTyr35 are replaced by water-mediated contacts in oxy-HbA (Park *et al.*, 2006).

4. Conclusions

The application of neutron protein crystallography is still limited, with the structures of relatively few proteins available to date. However, its role in building the structure–function relationship for enzymatic and functional proteins is increasing at a steady pace (Blakeley *et al.*, 2008). The current neutron structure of deoxy-HbA is the first to directly deter-

mine the protonation states of virtually all of the histidine residues that are vital for the ability of the protein to capture and release H^+. This information will help us to better understand the atomic mechanism of the Bohr effect and the overall function of HbA. Nevertheless, to reveal the role of each histidine a neutron structure of HbA in the oxy form would be essential. Based on our observations, we propose that the distal αHis58 and βHis63 residues and the buried histidines αHis103 may contribute to the macroscopic Bohr effect. We also found that the $\alpha_2\beta_2$ heterodimer was most likely not to be in the pure T state, based on the observations of the deprotonation and protonation of β_2His146 and β_2His143, respectively, and also of the differences in the protonation states of distal histidines compared with our previous neutron analysis. The current neutron structure also provided important information about the interactions between subunits, which are crucial for the stability of the T state.

This work was supported in part by Grants-in-Aid for Scientific Research from the Ministry of Education, Culture, Sports, Science and Technology of Japan (No. 17053011 to YM and No. 18790030 to TC) and grants from the REIMEI Research Resources of Japan Atomic Energy Research Institute (to YM) and Hyogo Science and Technology (to YM). The PCS is funded by the Office of Biological and Environmental Research of the Department of Energy. MM and PL were partly supported by an NIH–NIGMS-funded consortium (1R01GM071939-01) between LANL and LNBL to develop computational tools for neutron protein crystallography. AYK and PL were partly supported by a LANL LDRD grant (20070131ER).

References

Adams, P. D., Mustyakimov, M., Afonine, P. V. & Langan, P. (2009). *Acta Cryst.* D**65**, 567–573.
Bennett, B. C., Gardberg, A. S., Blair, M. D. & Dealwis, C. G. (2008). *Acta Cryst.* D**64**, 764–783.
Berenbrink, M. (2006). *Resp. Physiol. Neurobiol.* **154**, 165–184.
Blakeley, M. P. (2009). *Crystallogr. Rev.* **15**, 157–218.
Blakeley, M. P., Langan, P., Niimura, N. & Podjarny, A. (2008). *Curr. Opin. Struct. Biol.* **18**, 593–600.
Busch, M. R. & Ho, C. (1990). *Biophys. Chem.* **37**, 313–322.
Busch, M. R., Mace, J. E., Ho, N. T. & Ho, C. (1991). *Biochemistry*, **30**, 1865–1877.
Cera, E. D., Doyle, M. L. & Gill, S. J. (1988). *J. Mol. Biol.* **200**, 593–599.
Chatake, T., Shibayama, N., Park, S.-Y., Kurihara, K., Tamada, T., Tanaka, I., Niimura, N., Kuroki, R. & Morimoto, Y. (2007). *J. Am. Chem. Soc.* **129**, 14840–14841.
Collaborative Computational Project, Number 4 (1994). *Acta Cryst.* D**50**, 760–763.
Englander, J. J. & Englander, S. W. (1987). *Biochemistry*, **26**, 1846–1850.
Fang, T.-Y., Zou, M., Simplaceanu, V., Ho, N. T. & Ho, C. (1999). *Biochemistry*, **38**, 13423–13432.
Helliwell, J. R., Habash, J., Cruickshank, D. W. J., Harding, M. M., Greenhough, T. J., Campbell, J. W., Clifton, I. J., Elder, M., Machin, P. A., Papiz, M. Z. & Zurek, S. (1989). *J. Appl. Cryst.* **22**, 483–497.
Ho, C. & Russu, I. M. (1987). *Biochemistry*, **26**, 6299–6305.
Ikeda-Saito, M., Iizuka, T., Yamamoto, H., Kayne, F. J. & Yonetani, T. (1977). *J. Biol. Chem.* **252**, 4882–4887.
Imai, K., Fushitani, K., Miazaki, G., Ishimori, K., Kitagawa, T., Wada, Y., Morimoto, H., Morishima, I., Shih, D. T. & Tame, J. (1991). *J. Mol. Biol.* **218**, 769–778.
Ishimori, K., Imai, K., Miyazaki, G., Kitagawa, T., Wada, Y., Morimoto, H. & Morishima, I. (1992). *Biochemistry*, **31**, 3256–3264.
Kovalevsky, A. Y., Chatake, T., Shibayama, N., Park, S.-Y., Ishikawa, T., Mustyakimov, M., Fisher, S. Z., Langan, P. & Morimoto, Y. (2008). *Acta Cryst.* F**64**, 270–273.
Kovalevsky, A. Y., Chatake, T., Shibayama, N., Park, S.-Y., Ishikawa, T., Mustyakimov, M., Fisher, S. Z., Langan, P. & Morimoto, Y. (2010). *J. Mol. Biol.* **398**, 276–291.
Langan, P., Fisher, Z., Kovalevsky, A., Mustyakimov, M., Sutcliffe Valone, A., Unkefer, C., Waltman, M. J., Coates, L., Adams, P. D., Afonine, P. V., Bennett, B., Dealwis, C. & Schoenborn, B. P. (2008). *J. Synchrotron Rad.* **15**, 215–218.
Langan, P., Greene, G. & Schoenborn, B. P. (2004). *J. Appl. Cryst.* **37**, 24–31.
Matthew, J. B., Gurd, F. R. N., Garcia-Moreno, B., Flanagan, M. A., March, K. L. & Shire, S. J. (1985). *CRC Crit. Rev. Biochem.* **18**, 91–197.
Monod, J., Wyman, J. & Changeux, J.-P. (1965). *J. Mol. Biol.* **12**, 88–118.
Park, S.-Y., Yokoyama, T., Shibayama, N., Shiro, Y. & Tame, J. R. H. (2006). *J. Mol. Biol.* **360**, 690–701.
Perutz, M. F. (1970). *Nature (London)*, **228**, 726–739.
Perutz, M. F. (1989). *Q. Rev. Biophys.* **22**, 139–287.
Perutz, M. F., Fermi, G., Luisi, B., Shaanan, B. & Liddington, R. C. (1987). *Acc. Chem. Res.* **20**, 309–321.
Perutz, M. F., Gronenborn, A. M., Clore, G. M., Fogg, J. H. & Shih, D. T. (1985). *J. Mol. Biol.* **183**, 491–498.
Perutz, M. F., Kilmartin, J. V., Nishikura, K., Fogg, J. H., Butler, P. J. G. & Rollema, H. S. (1980). *J. Mol. Biol.* **138**, 649–670.
Perutz, M. F., Wilkinson, A. J., Paoli, M. & Dodson, G. G. (1998). *Annu. Rev. Biophys. Struct.* **27**, 1–34.
Pflugrath, J. W. (1999). *Acta Cryst.* D**55**, 1718–1725.
Pintar, A. & Pongor, S. (2003). *Bioinformatics*, **19**, 313–314.
Rao, M. J. & Acharya, A. S. (1992). *Biochemistry*, **31**, 7231–7236.
Riggs, A. F. (1988). *Annu. Rev. Physiol.* **50**, 181–204.
Russu, I. M., Wu, S.-S., Ho, N. T., Kellogg, G. W. & Ho, C. (1989). *Biochemistry*, **28**, 5298–5306.
Shibayama, N., Imai, K., Hirata, H., Hiraiwa, H., Morimoto, H. & Saigo, S. (1991). *Biochemistry*, **30**, 8158–8165.
Shih, D. T. & Perutz, M. F. (1987). *J. Mol. Biol.* **195**, 419–422.
Sun, D. P., Zou, M., Ho, N. T. & Ho, C. (1997). *Biochemistry*, **36**, 6663–6673.
Tsuneshige, A., Park, S. & Yonetani, T. (2002). *Biophys. Chem.* **98**, 49–63.
Wyman, J. (1964). *Adv. Protein Chem.* **19**, 223–286.
Yang, F. & Phillips, G. N. Jr (1996). *J. Mol. Biol.* **256**, 762–774.
Yonetani, T., Park, S., Tsuneshige, A., Imai, K. & Kanaori, K. (2002). *J. Biol. Chem.* **277**, 34508–34520.